ResearchGate

See discussions, stats, and author profiles for this publication at: https://www.researchgate.net/publication/257325204

Nanosized Ce1−xLaxO2−δ/Al2O3 solid solutions for CO oxidation: Combined study of structural characteristics and catalytic evaluation

ARTICLE *in* CATALYSIS TODAY · DECEMBER 2012

Impact Factor: 3.89 · DOI: 10.1016/j.cattod.2012.07.015

CITATIONS
10

READS
16

4 AUTHORS, INCLUDING:

Benjaram M Reddy
CSIR-Indian Institute of Chemical Technology
279 PUBLICATIONS **5,650** CITATIONS

SEE PROFILE

All in-text references underlined in blue are linked to publications on ResearchGate, letting you access and read them immediately.

Available from: Benjaram M Reddy
Retrieved on: 24 January 2016

Provided for non-commercial research and education use.
Not for reproduction, distribution or commercial use.

This article appeared in a journal published by Elsevier. The attached copy is furnished to the author for internal non-commercial research and education use, including for instruction at the authors institution and sharing with colleagues.

Other uses, including reproduction and distribution, or selling or licensing copies, or posting to personal, institutional or third party websites are prohibited.

In most cases authors are permitted to post their version of the article (e.g. in Word or Tex form) to their personal website or institutional repository. Authors requiring further information regarding Elsevier's archiving and manuscript policies are encouraged to visit:

http://www.elsevier.com/copyright

Author's personal copy

Catalysis Today 198 (2012) 133–139

Contents lists available at SciVerse ScienceDirect

Catalysis Today

journal homepage: www.elsevier.com/locate/cattod

Nanosized $Ce_{1-x}La_xO_{2-\delta}/Al_2O_3$ solid solutions for CO oxidation: Combined study of structural characteristics and catalytic evaluation

Lakshmi Katta, T. Vinod Kumar, D. Naga Durgasri, Benjaram M. Reddy*

Inorganic and Physical Chemistry Division, Indian Institute of Chemical Technology, Uppal Road, Hyderabad 500 607, India

ARTICLE INFO

Article history:
Received 22 February 2012
Received in revised form 10 July 2012
Accepted 12 July 2012
Available online 24 August 2012

Keywords:
Ceria–lanthana
Alumina support
Solid solution
Catalyst characterization
Oxygen storage capacity
CO oxidation

ABSTRACT

Nanosized lanthanum-doped ceria ($Ce_{1-x}La_xO_{2-\delta}$) and the same dispersed on alumina support ($Ce_{1-x}La_xO_{2-\delta}/Al_2O_3$) were synthesized following a simple and high yielding procedure. Formation of solid solutions and interaction with the support were monitored by X-ray diffraction (XRD), Raman spectroscopy (RS; UV-RS and Vis-RS), high-resolution electron microscopy (HREM), Brunauer–Emmett–Teller (BET) surface area, X-ray photoelectron spectroscopy (XPS), temperature programmed reduction (TPR) and diffuse reflectance spectroscopy (UV-DRS) techniques. XRD results confirmed the formation of ceria–lanthana solid solutions. HREM studies revealed well distributed and small sized Ce–La–oxide particles of ~7 nm size over the surface of alumina support. Formation of defect sites or oxygen vacancies was investigated by RS using 325 and 632.81 nm excitation laser lines which confirmed their presence in the investigated samples. RS studies further deduced that evolution of oxygen vacancies (~570 cm^{-1}) was due to different ionic valence state of dopant (La^{3+}) from that of Ce^{4+}, while the development of MO_8-type complex (~600 cm^{-1}) was due to different ionic radius of dopant (La^{3+}, 0.110 nm) from that of Ce^{4+} (0.097 nm). XPS results suggested that there is no significant change in the Ce^{3+} amount during thermal treatments due to the absence of undesirable cerium aluminates formation. TPR data revealed that surface modification with support enhances the reducibility of the doped ceria. Catalytic evaluation showed a 50% CO conversion temperature of 634 K per 66 mg of CL for the CL/A catalyst, which is lower than the CL sample (636 K per 100 mg of CL), possibly on account of an increased dispersion, more oxygen vacancies and easy reducibility.

© 2012 Elsevier B.V. All rights reserved.

1. Introduction

The environmental legislation has imposed stringent targets for permitted levels of atmospheric emissions. The removal of detrimental gases (CO, NO_x, HC, etc.) from the automobile exhausts is therefore an immense commendable task. Among these, the complete oxidation of carbon monoxide is of prime importance to meet increasingly stringent environmental regulations in a practical way. The catalysts being mostly studied for these processes are supported Pd, Pt and Rh based catalysts; however, the rarity and cost of these catalysts are posing serious problems to the implementation of clean energy technologies on a large scale. Therefore, there is an ongoing search for inexpensive and highly active catalysts for CO oxidation and other related applications [1].

Ceria (CeO_2) has long been regarded as one of the key materials in modern catalysis due to its ability to cycle easily between reduced and oxidized states (i.e. $Ce^{3+} \leftrightarrow Ce^{4+}$) in combination with numerous oxygen vacancies [2–5]. This eminent feature has been considered as the heart of the material which makes present automotive exhaust treatment catalysts containing ceria much more effective than their predecessors. Further, nanosized ceria has been reported to be active for free-radical scavenging and oxidase-like activity in bio-systems [6,7]. Recently, it has also been employed as a redox catalyst for thermochemical production of chemicals using solar energy [8]. However, pure ceria is poorly thermostable and undergoes rapid sintering under high-temperature conditions thereby loses its crucial oxygen storage/release capacity (OSC). The most important strategy to tackle this problem is to modify ceria with other elements. The key parameters that are important when doping the ceria with any other oxide are (i) the dopant ion concentration and (ii) size and/valance of the dopant ion to achieve optimum reducibility [5]. With respect to undoped oxide, doped ceria with cations of different size or charge alter ion mobility inside the modified lattice, resulting in the formation of non-stoichiometric defective fluorite-structured solid solutions. Such amendments in the defect structure of ceria confer new properties to the catalyst such as better resistance to sintering at high temperatures and a decrease in the activation energy for oxygen vacancy formation during reduction. Thus, incorporation of appropriate dopants into the ceria lattice results in the formation of new

* Corresponding author. Tel.: +91 40 2719 1714; fax: +91 40 2716 0921.
E-mail addresses: bmreddy@iict.res.in, mreddyb@yahoo.com (B.M. Reddy).

0920-5861/$ – see front matter © 2012 Elsevier B.V. All rights reserved.
http://dx.doi.org/10.1016/j.cattod.2012.07.015

Author's personal copy

stable compounds leading to different physicochemical properties and catalytic behavior [9,10].

Among various dopants, lanthana has attracted considerable attention recently. Mackrodt et al. first observed a noticeable improvement in the catalytic activity of ceria–lanthana solid solutions for combustion of methane [11]. Lanthanum and cerium are the nearest homologous elements and both belong to lanthanide series, which exhibit fine chemical toning property [12]. However, a large difference in the ionic radii between La^{3+} and Ce^{4+} is expected to induce huge lattice deformation and promote the oxygen vacancy (charge compensation mechanism) generation in the ceria lattice which can facilitate more channels for oxygen flow, together serve as key factors for oxidation reactions. To further increase the surface area and to sustain high activity under real conditions, ceria-based systems are usually supported on transition aluminas (~127 m^2/g), with the aim of achieving good dispersion of the active phase and enhancement in the oxygen exchange rate.

The present investigation was undertaken against the aforesaid background. Accordingly, the primary goal of the present study was to understand the influence of support on the catalytic activity of La^{3+} doped ceria. For this purpose, nanosized $Ce_{1-x}La_xO_{2-\delta}$ (CL) and $Ce_{1-x}La_xO_{2-\delta}/Al_2O_3$ (CL/A) solid solutions were synthesized by coprecipitation and deposition coprecipitation methods, respectively and evaluated for CO oxidation. The physicochemical properties were investigated by using a variety of techniques including Brunauer–Emmett–Teller (BET) surface area, X-ray diffraction (XRD), X-ray photoelectron spectroscopy (XPS), transmission electron microscopy (TEM), UV–visible diffuse reflectance spectroscopy (UV–vis DRS), Raman spectroscopy and temperature programmed reduction (H_2-TPR).

2. Experimental

2.1. Catalyst preparation

The investigated ceria–lanthana (CL; 8:2 mole ratio based on oxides) and ceria–lanthana/alumina (CL/A; 8:2:10 mole ratio based on oxides) samples were prepared by coprecipitation and deposition coprecipitation methods, respectively using cerium(III) nitrate (Aldrich, AR grade) and lanthanum(III) nitrate (Aldrich, AR grade) precursors. At first, the desired quantity of powdered γ-alumina (Harshaw, specific surface area ~127 m^2/g) was dispersed in about 2000 ml of deionized water and stirred for 2 h. Requisite amounts of cerium and lanthanum precursors were dissolved separately in 500 ml of deionized water, mixed together and stirred continuously for 1 h. Under stirring conditions, the nitrate precursor solutions and the dispersed alumina solution were thoroughly mixed and the whole mixture was diluted to 4000 ml with deionized water. Upon completion of mixing, an excess amount of ultra diluted ammonium hydroxide was added dropwise resulting in a pH of ~8.5. The obtained precipitates were filtered off and washed several times with deionized water until free from anion impurities. The obtained cake was oven-dried at 393 K for 12 h and calcined at 773 K for 5 h. The calcined mixed oxides were once again heated at 873, 973 and 1073 K for 5 h. For comparison, ceria sample was also prepared following the same procedure under identical conditions.

2.2. Catalyst characterization

XRD data was acquired in the 2θ range of 12–80° on a Rigaku Multiflex instrument using Cu Kα (λ = 1.5418 Å) radiation and a scintillation counter detector. The average crystallite size of CL and CL/A samples were estimated with the help of Debye–Scherrer equation using the XRD data of all prominent lines, and the cell parameter '*a*' was calculated by a standard cubic indexation method using the intensity of the base peak (1 1 1) [13,14]. High-resolution electron microscopy (HREM) studies were made on a JEM-2010 (JEOL) instrument equipped with a slow-scan CCD camera and at an accelerating voltage of 200 kV. The Raman spectra were obtained at room temperature using a LabRam HR800UV Raman spectrometer (Horiba Jobin-Yvon) fitted with a confocal microscope and liquid-nitrogen cooled charge-coupled device (CCD) detector. The BET surface areas were determined by adsorption isotherms at liquid N_2 temperature (77 K) recorded on SMART SORB–92/93 instrument via a thermal conductivity detector. The XPS measurements were performed on a Shimadzu (ESCA 3400) spectrometer by using Mg Kα (1253.6 eV) radiation as the excitation source. Charging of catalyst samples was corrected by setting the binding energy of the adventitious carbon (C 1s) at 284.6 eV. The XPS analysis was done at ambient temperature and pressures usually in the order of less than 10^{-8} Pa. The UV–vis DRS measurements were conducted over the wavelength range of λ = 200–750 nm using a GBS-Cintra 10e UV–vis NIR spectrophotometer with an integration sphere diffuse reflectance attachment. Sample was diluted in a KBr matrix by pelletization. Reducibility of the samples was examined by H_2-TPR using thermal conductivity detector of a gas chromatograph (Shimadzu) in a conventional lab apparatus. About 30 mg of sample mass was loaded in an isothermal zone of the reactor and heated at a rate of 10 K/min to 473 K using 30 ml/min helium gas flow which facilitated to drive away the molecules that had been pre-adsorbed on the surface of the catalysts. After the sample was cooled to room temperature, the helium was switched to 5% H_2/Ar with a rate of 20 ml/min and the temperature was linearly raised to 1073 K at a continuous heating ramp of 5 K/min. The hydrogen consumption during the reduction process was calculated by passing the effluent gas through a molecular sieve trap to remove the produced water and then to TCD.

2.3. Catalyst evaluation

The catalytic performance of the sample for CO oxidation was conducted at normal pressure in the temperature range 300–773 K @ 5 K/min using a fixed bed reactor of micro activity. About 100 mg catalyst sample (250–355 μm sieve fraction) was diluted with quartz particles of the same sieve fraction and placed in a quartz reactor. The total flow rates (9.98% CO and 10.2% O_2 balanced with argon) maintained by three mass flow controllers were in the range of 50–60 sccm (standard cubic centimeters per minute). The CO and CO_2 gas concentrations were measured using an Uras 14 infrared analyzer module, and the O_2 concentration was measured using a Magnos 16 analyzer (Hartmann & Braun). Prior to oxidation of CO, the catalyst was heated to 773 K in 10.2% O_2/Ar gas mixture, using a heating ramp of 10 K/min, and kept at the final temperature for 1 h. Then the oxidized sample was purged in argon. Partial pressures of CO and O_2 were in the range of 10 mbar.

3. Results and discussion

XRD analysis provides information corresponding to crystallographic structure, structural deformation, solid solution formation and crystallite size of the oxide samples. The XRD patterns of CL and CL/A samples calcined at 773 K and 1073 K are presented in Figs. 1 and 2, respectively. For comparison purpose, the diffractograms of pure ceria (C) and γ-alumina (A) are also included. From the figures, it is clear that all samples show highly symmetric, well-defined patterns and could be indexed as (1 1 1), (2 0 0), (2 2 0), (3 1 1), (2 2 2), (4 0 0), (3 3 1) and (4 2 0), which clearly manifest the peaks characteristic of the fluorite type cubic structure. No reflections from other planes related to lanthana, γ-alumina

Author's personal copy

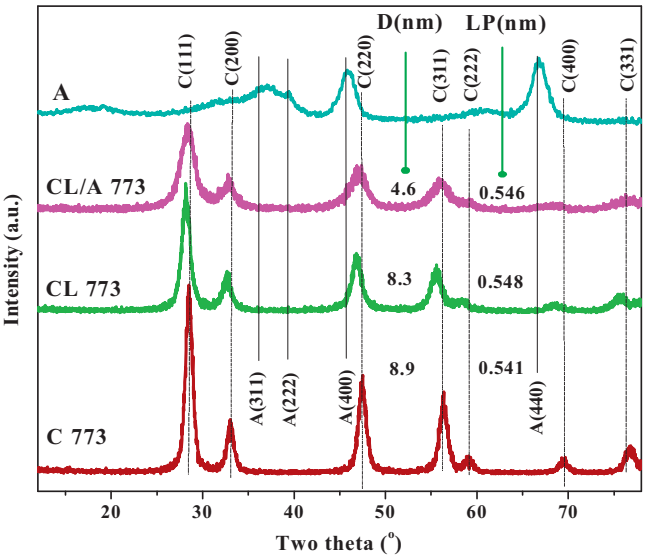

Fig. 1. Powder XRD patterns of alumina supported ceria–lanthana (CL/A), ceria–lanthana (CL), γ-alumina (A) and pure ceria (C) calcined at 773 K.

and cerium aluminates are observed. Absence of any peak related to lanthana unveiled the successful incorporation of La^{3+} ions into the ceria lattice and the formation solid solution. The lattice parameter and mean crystallite size values are given in the figures. The introduction of heavier metal ion (La^{3+}, ~0.110 nm) into the Oh environment of ceria lattice (Ce^{4+}, ~0.097 nm) induces strain in the ceria matrix that result in an increase in the lattice parameter approximately 0.078 Å (5.410–5.488 Å), which is due to the repulsion between the extra-interstitial anions accompanying the substitution of La^{3+} by Ce^{4+} [15]. The change in the lattice parameter values and peak broadening are more prominent with alumina support. The more broadening in case of CL/A sample than that of CL is due to the decrease in the crystallite size as well as the presence of crystal defects. The change in the lattice parameter for CL/A sample is evidenced from a small shift in the peak positions to higher angles compared to CL. The shift in the peak positions supports the assumption that there is a specific interaction between various

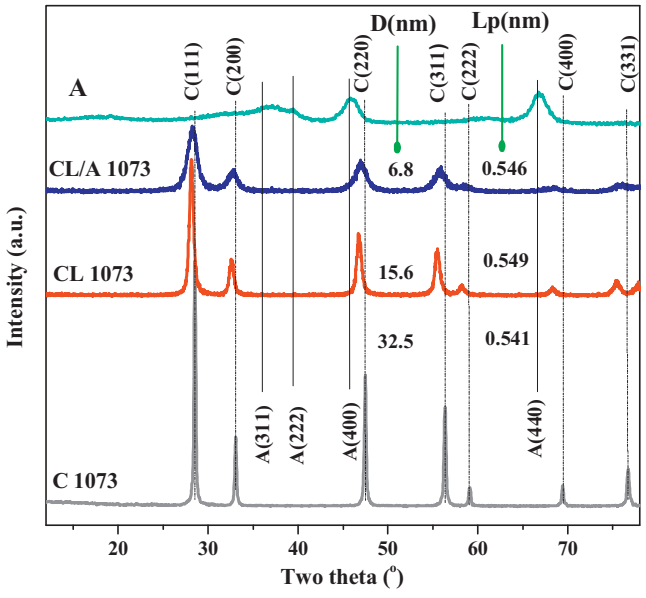

Fig. 2. Powder XRD patterns of alumina supported ceria–lanthana (CL/A), ceria–lanthana (CL), γ-alumina (A) and pure ceria (C) calcined at 1073 K.

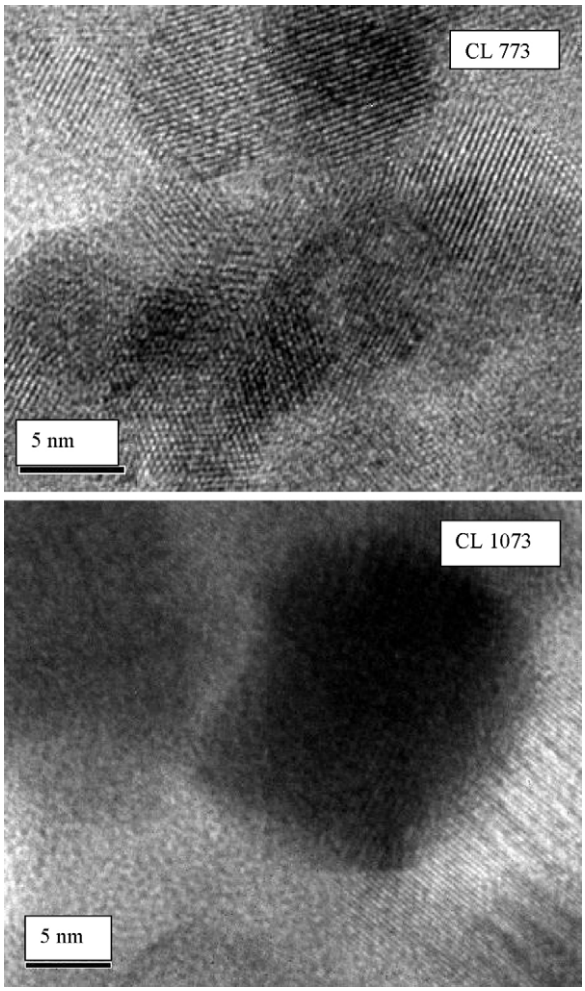

Fig. 3. HREM micrographs of ceria–lanthana (CL) calcined at 773 and 1073 K.

component oxides. The absence of peaks corresponding to alumina support and $CeAlO_3$ mixed compound could be due to the presence of support in amorphous form and the presence of lanthana as a promoter that inhibits the undesirable interaction between ceria and alumina, respectively [16].

The decrease in the crystallite size due to microstrain effects [17] goaded by the expansion of lattice parameter are due to the presence of trivalent lanthana cations in the ceria structure. From the crystallite size values, it is clear that the effect of temperature is different from ceria to CL/A. Pure ceria encounter with high crystallite growth (8.9–32.5 nm), and incorporation of La^{3+} ions hinders such sintering (8.3–15.6 nm). Crystallite sizes of the supported samples are still lowered and fall in the 4–7 nm range for 773–1073 K temperatures. Surface area of the CL is significantly increased (increased from 66 to 108 m^2/g at 773 K) when it was dispersed on high surface area support because of fine dispersion. The surface area order is as follows: C < CL < CL/A at both 773 and 1073 K. With increase in the calcination temperature surface area decreases and crystallite size increases due to sintering, but the values are moderate in the case of CL/A compared to the values of the CL sample, which invokes the importance of the support.

The HREM micrographs of CL and CL/A samples calcined at 773 and 1073 K are presented in the Figs. 3 and 4, respectively. Nanoparticles of all the samples appeared as if they are uniformly distributed and weakly aggregated. Particularly, the HREM pictures of CL/A sample consist of distinct crystallites with strong faceting and well-defined edges, and these structural characteristics are

Author's personal copy

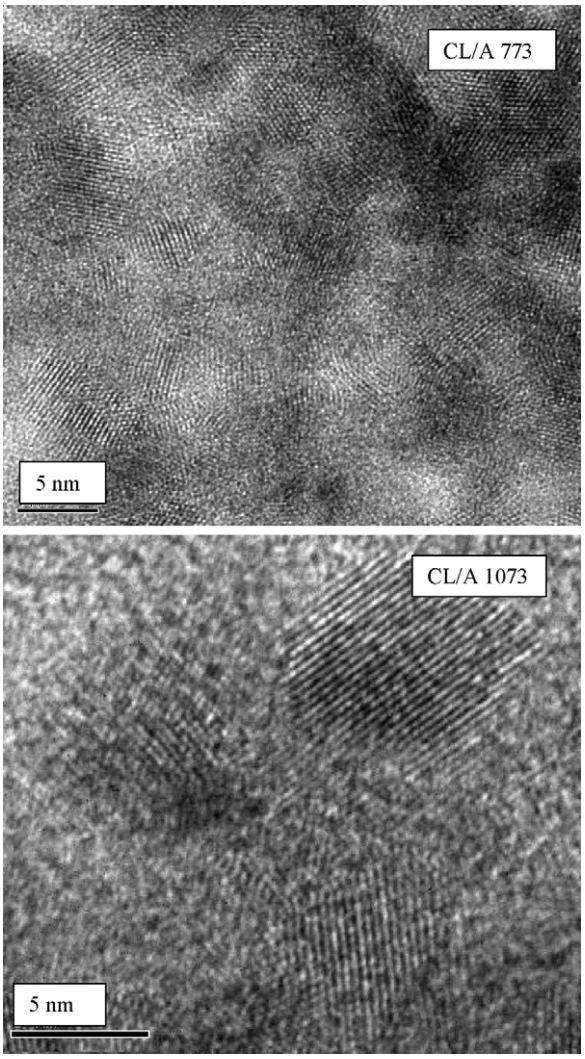

Fig. 4. HREM micrographs of alumina supported ceria–lanthana (CL/A) calcined at 773 and 1073 K.

attractive for catalysis point of view. The clearly visible lattice fringes provide evidence for high degree of crystallinity within the domains and the observations revealed that the particles are well dispersed in CL/A compared to CL. The patterns of the two catalysts clearly indicated that the particles of CL are larger than the supported CL sample. It is worth mentioning here that the aggregation of the material increases with calcination temperature and is less in the supported CL sample which could be explained based on the diffusion barrier concept [18].

Raman spectroscopy (RS) is an excellent, nondestructive and rapid analysis technique for investigating the electronic and phonon structure of materials. RS in combination with the XRD is often introduced to distinguish the formation of solid solutions from the individual oxides. Figs. 5 and 6 show the RS of pure ceria, CL and CL/A samples obtained with two excitation laser lines 325 and 632.81 nm, respectively. The spectra obtained at the UV-region provide the information about near to surface region due to the strong absorption of samples, and the spectra obtained at the visible region reflect both surface and bulk information due to the weak absorption of the samples. Generally, RS of ceria-based materials furnish three probable bands: an intense band at 464 cm^{-1}, and the faint humps at 570 cm^{-1} and/or at 600 cm^{-1}. The former band has been assigned as F_{2g} mode (α) characteristic of ceria (the only allowed in first order) [19]. This band corresponds to the oxygen

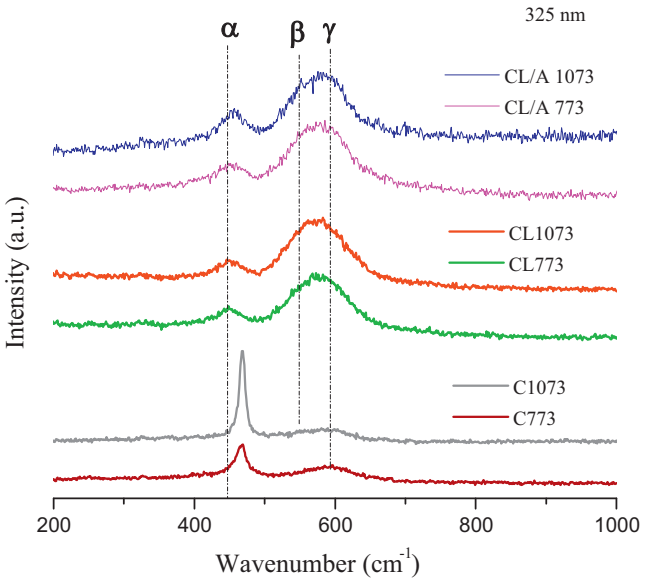

Fig. 5. UV-Raman spectra of alumina supported ceria–lanthana (CL/A), ceria–lanthana (CL) and pure ceria (C) calcined at 773 and 1073 K.

breathing vibrations around Ce^{4+} and it is sensitive to several factors, such as phonon confinement, strain, inhomogeneity of the size distribution, defects and variations in the phonon relaxation with the particle size. Normally, doping of ceria affects the polarizability of the symmetrical stretching mode of [$Ce–O_8$] vibrational unit, thereby leads to the broadening along with a logical shift in the F_{2g} band [19].

In comparison to pure ceria, the F_{2g} band of La^{3+} doped ceria become weaker which is in good agreement with the previous reports [20]. Also, the octahedral void in the ceria lattice is enlarged which modifies the MO vibrations. The shift could be attributed to large ionic radii of La^{3+} dopant ion. The peak corresponding to lanthana phase is not observed (generally, observed at ~405 cm^{-1} attributed to torsional skeleton mode of hexagonal units) due to the formation of solid solution which is in line with the XRD results [21]. As seen from both UV- and vis- RS, a little shift in the F_{2g} band position of CL/A to higher energy is identified compared to CL which

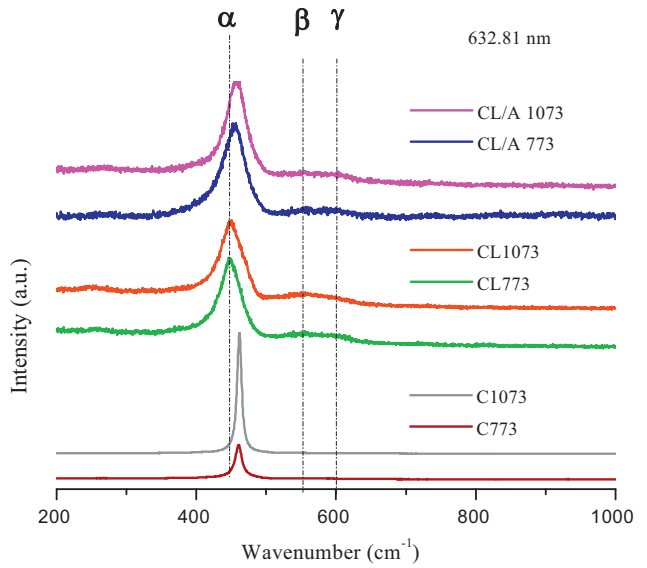

Fig. 6. Visible-Raman spectra of alumina supported ceria–lanthana (CL/A), ceria–lanthana (CL) and pure ceria (C) calcined at 773 and 1073 K.

Author's personal copy

is payable to slight increment in the MO vibration. The decrease in the lattice parameter (noted from XRD) together with the increment in the MO vibrations account for small amount of lanthana that could come out of the lattice and acts as effective barrier for the undesirable interactions, generally observed for alumina supported ceria samples [18].

The appearance of latter bands (570 or 600 cm^{-1}) is certainly dependent on the valance and size of the dopant used. To the best of our knowledge, the band at 570 cm^{-1} (β) was found for the first time in the work of Nakajima et al. that can be ascribed to the oxygen vacancies introduced into the ceria lattice in order to maintain charge neutrality when Ce^{4+} ions are replaced with lower valent cations [22]. It has been demonstrated that the lattice strain increases with the lower valent La^{3+} dopant ion as a result of generation of oxygen vacancies at the expense of charge. The 600 cm^{-1} (γ) is attributed to Oh symmetry that include a dopant cation in the 8-fold coordination of O^{2-} (MO_8-type complex) but did not contain any oxygen vacancies. It was found that the evolution of oxygen vacancies are due to a different valence state of dopant from that of Ce^{4+}, while the evolution of the MO_8-type complex was due to different ionic radius of dopant from that of Ce^{4+}. As seen from the figures, for CL and CL/A samples, these two frequencies merged as an extended broad band in the UV-RS, but are clearly resolved in the Vis-RS.

From the Fig. 5, it is clear that the spectra recorded at UV-region, the peaks for the oxygen vacancies as well as MO_8-type complex are relatively stronger than F_{2g} band, but those taken at visible laser line (Fig. 6) are weaker than the F_{2g} band. This disparate feature could be attributed to the enrichment of the defects on the surface of the material. Compared to pure ceria, the areas under the peaks for CL and CL/A at above-mentioned frequencies are more, which indicate that the concentration of oxygen vacancies and MO_8 complex defects (intrinsic oxygen vacancies) are enhanced in the CL and CL/A samples. The increase of oxygen vacancy concentration in CL and CL/A samples could facilitate more channels for the exchange of oxygen, which benefit in improving the OSC of ceria-based materials. With increase in the calcination temperature, the intensity of the peaks corresponding to 570 and 600 cm^{-1} is decreased in vis-RS. Conversely, in UV-RS a meager increase and decrease in the intensity of the peaks at 570 and 600 cm^{-1}, respectively is noted. This observation indicates that the concentration of oxygen vacancies is slightly increased and MO_8-type complex defect slightly decreased at the near surface region. These are essentially related to ordering level of the sample which is increased with temperature [19,23].

To examine the chemical states of the dopant and the host ions on the surface of the ceria-based solid solutions, XPS study was carried out. The spectra of ceria are intricate and split into Ce $3d_{3/2}$ and Ce $3d_{5/2}$ with multiple shake-up and shake-down satellites. The bands v_0, v, v′, v″ and v‴ are ascribed to the Ce $3d_{5/2}$ ionization, while u_0, u, u′, u″ and u‴ are assigned to Ce $3d_{3/2}$ ionization. The u‴/v‴ doublet is due to the primary photoemission from $Ce(IV)O_2$. The u′/v′ doublet is due to Ce(III) cations. The Ce 3d spectrum of all the samples gives rise to a myriad of peaks basically stands for a mixture of Ce^{3+}/Ce^{4+} oxidation states indicating that the surface of the sample is not fully oxidized. From Fig. 7, it is understandable that the intensity of the peaks pertaining to u‴ is increased, simultaneously a progressive reduction in the intensity of v_0/u_0 and v′/u′ is noted for CL/A sample compared to unsupported CL that denotes a decrement in Ce^{3+} concentration over the surface. This observation revealed that the presence of La minimizes the interaction between Ce and Al responsible for the formation of cerium aluminates where Ce is present in 3+ oxidation state [24].

In general, the peaks corresponding to the O 1s (Fig. 8) are broad and complicated because of the nonequivalence of surface oxygen ions. The peak shape suggests that it is composed of more than one peak arising from the overlapping contribution of oxygen from rare

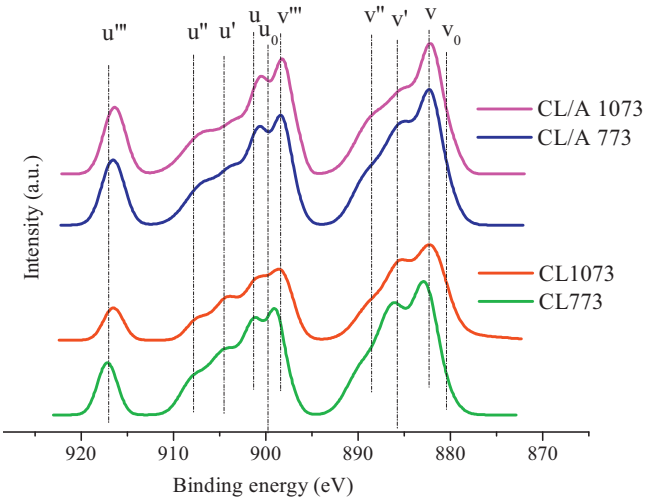

Fig. 7. Ce 3d XPS patterns of alumina supported ceria–lanthana (CL/A) and ceria–lanthana (CL) calcined at 773 and 1073 K.

earth oxide, alumina, mixture of hydroxyl contamination, adsorbed oxygen species, carbonate contamination and highly polarized oxygen anions close to a vacancy center [25]. The appearance of peak at low binding energy around ~529 eV is typical of lattice oxygen of CeO_2, Ce_2O_3 and La_2O_3 oxides. The component peak at around ~531 eV is due to the presence of support and is characterized by Al—O bond. The origin of high binding energy (~532 eV) peak is owing to combination of hydroxyl and carbonate contamination on the surface of the material. It is difficult to rationalize the high binding energy feature to contamination or adsorbed oxygen, since the sample changes from a state of almost entirely Ce^{3+} to Ce^{4+}. As the calcination temperature increased, the intensity of this particular peak is decreased due to removal of surface residues [26].

UV–vis DRS technique is more useful to investigate the metal oxides with nanocrystalline nature which escape from the XRD detection. The spectra of all the samples are presented in Fig. 9. The characteristic absorption bands at 255, 290 and 346 nm are corresponding to the $O^{2-} \rightarrow Ce^{3+}$ and $O^{2-} \rightarrow Ce^{4+}$ ligand to metal charge transfer (LMCT) and interband transitions (IBT), respectively [27]. As known, the $O^{2-} \rightarrow Ce^{3+}$ represents defects produced in the lattice during the incorporation of dopant as well as support formation which is well resolved for CL/A compared to pure ceria. Similar

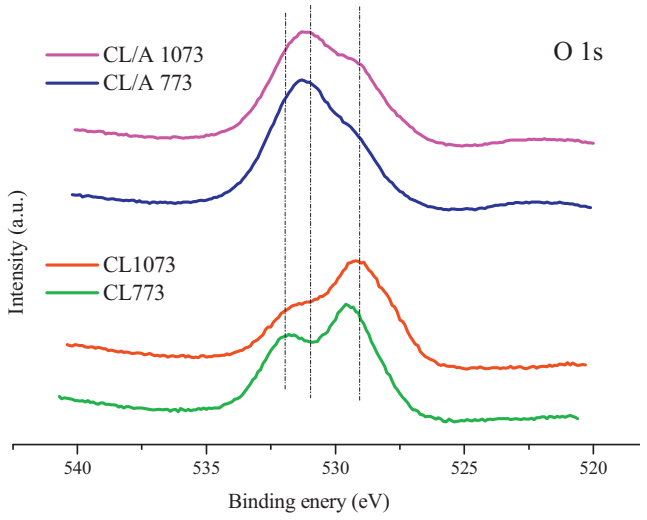

Fig. 8. O 1s patterns of alumina supported ceria–lanthana (CL/A) and ceria–lanthana (CL) calcined at 773 and 1073 K.

Author's personal copy

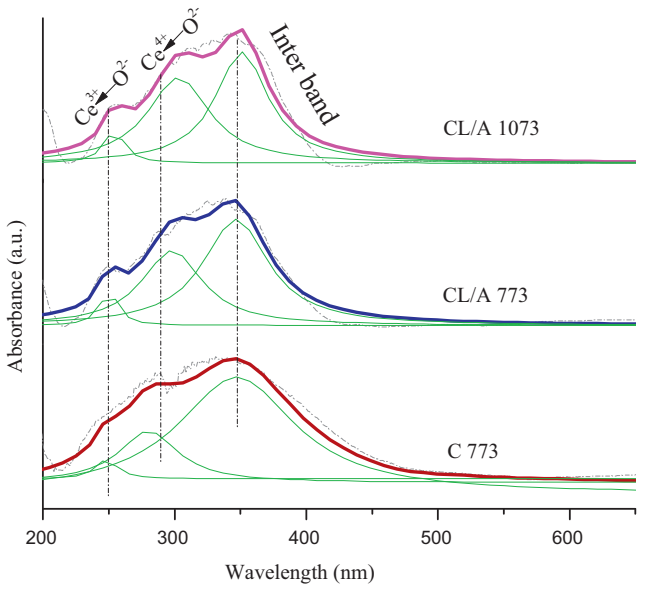

Fig. 9. UV–vis DRS of ceria (C) calcined at 773 K and alumina supported ceria–lanthana (CL/A) at 773 and 1073 K.

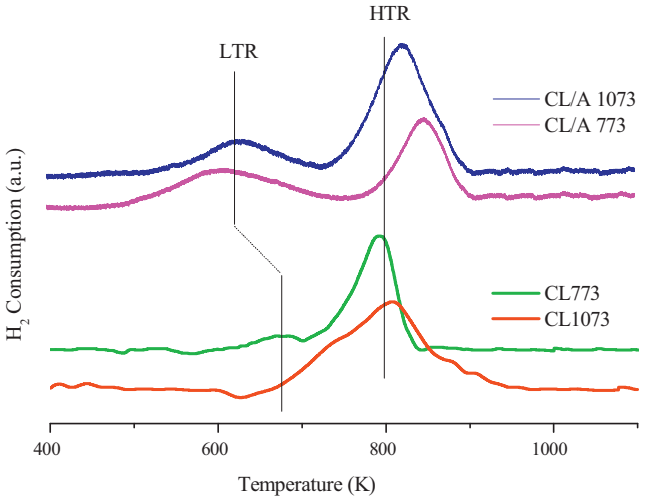

Fig. 10. TPR patterns of alumina supported ceria–lanthana (CL/A) and ceria–lanthana (CL) calcined at 773 and 1073 K.

to the previous studies, CL/A sample has also shown an increasing blue shift of the absorption edge and, consequently decrease in the average particle size related to bare ceria [28]. This fact has been proposed to arise as a consequence of either the quantum size effect originated by the diminution of ceria particle size, or the existence of larger contribution of $O^{2-} \rightarrow Ce^{4+}$ charge transfer transitions, which yield a relatively broad band with a maximum at ca. 380 nm.

The reducibility of CL and CL/A can be accomplished by monitoring the interaction of samples with H_2 at various temperatures by TPR. Generally the reduction for pure ceria proceeds via two steps. Low-temperature reduction (LTR) observed at ~790 K ascribed to surface and high temperature reduction (HTR) at ~1059 K reflects bulk oxide as known earlier [5]. The presence of dopant and support clearly promotes reduction of oxygen species as documented by the shift of the peak to the lower temperature [29,30]. In the case of CL solid solution, the peaks appeared at 671, 792 K and 740, 808 K for the samples calcined at 773 and 1073 K, whereas, for CL/A these are at 625, 606 K and 823, 848 K, respectively corresponding to surface and bulk reduction (Fig. 10).

The CO oxidation over ceria-based oxides is producing numerous and often conflicting models and mechanisms. For instance, CO oxidation is anticipated to proceed through two established paths: (i) Langmuir–Hinshelwood mechanism, where the reaction takes place between all adsorbed species on the catalyst surface and (ii) Mars–van-Krevelen (MVK) mechanism. Liu et al. confirmed using isotopic studies that CO oxidation majorly follows through the MVK mechanism [31,32]. It is often agreed that the lattice oxygen/oxygen vacancy plays an important role in the oxidation of CO. It has been reported that oxygen vacancy present in the ceria acts as the site to adsorb gaseous oxygen for the formation of active oxygen [31]. Formation of active oxygen and its utilization followed by the regeneration of oxygen vacancy would be the key processes for maintaining high catalytic activity.

The catalytic activity towards CO oxidation over CL and CL/A samples calcined at different temperatures are presented in Fig. 11. The oxidation of CO over all the samples is commenced below 550 K and the steady state is reached after 700 K. Therefore, the light-off-temperature (T_{50}) is taken into account to differentiate the activity. The increasing order of light-off temperature for CL and CL/A samples is as follows: CL/A 773 < CL 773 < CL/A 1073 < CL 1073. The T_{50} is found to be 636 K for CL 773 sample (per 100 mg of CL). Interestingly, the T_{50} for CL/A 773 is reached at 634 K (per 66 mg of CL; balanced with alumina). This observation indicates that the amount of catalytic active reducible species was greatly minimized in the presence of alumina support. Also, the difference between T_{50} and T_{100} for CL 773 is 143 K and for CL/A 773 is just 72 K. The limiting (T_{100}) CO oxidation was observed below 700 K in the case of CL/A 1073, whereas it is observed above 800 K for CL 1073. The foremost reason for the enhanced activity of CL/A could be due to the complex interactions that occur at the interface of mixed metal oxide and the support [33]. It has been reported earlier that interaction between metal oxide and support could be stronger than the metal and support interaction due to chemical bonding of the support that is more closely resembles to the supported oxide [34,35]. This phenomenon reduces undesirable interaction between alumina and ceria with subsequent enhancement in the reducibility of ceria that lead to a significant enhancement in the chemical reactivity. High

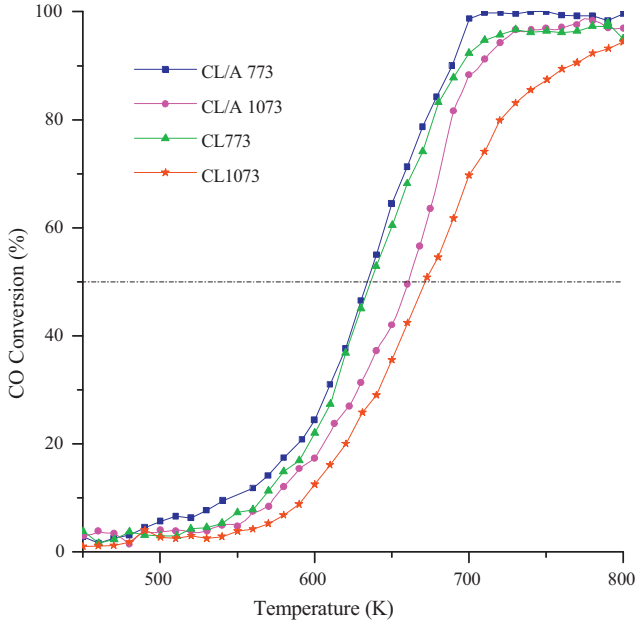

Fig. 11. Conversion of CO as a function of reaction temperature over alumina supported ceria–lanthana (CL/A) and ceria–lanthana (CL) calcined at 773 and 1073 K.

Author's personal copy

surface area and small crystallite size could also be the reasons for the excellent catalytic activity of CL/A over the CL sample.

4. Conclusions

Nanosized CL and CL/A materials with 8:2 and 8:2:10 (oxide ratio) compositions were prepared by coprecipitation and deposition coprecipitation methods, respectively. The effect of oxygen vacancies, crystallite size and surface area on the catalytic performance toward the CO oxidation reaction has been examined. The following observations were made from the current study:

(i) It was confirmed by XRD, Raman and XPS results that absence of undesirable interaction between Ce and Al invokes the superiority of the La promoter.
(ii) It was confirmed by TEM, BET surface area and TPR results that a high activity for CO oxidation in reaching the limiting value in the case of CL/A than CL is mainly due to the strong interaction of the support with the CL mixed oxide which provides more active sites for the adsorption of CO over the surface.

The enhanced catalytic activity of CL/A sample for oxidation reactions may be useful to diminish the amount of noble metals, which is one of the foremost important challenges for auto-exhaust catalysis.

Acknowledgements

We greatly acknowledge Prof. Dr. W. Grünert, RUB, Germany for providing CO oxidation results. We also thank Dr. Tetsuo Umegaki, AIST-Kansai, Japan for help in XPS measurements. L.K., T.V.K. and D.N.D. wish to thank the Council of Scientific and Industrial Research (CSIR), New Delhi for research fellowships. Financial support was received from Department of Science and Technology, New Delhi, under SERC Scheme (SR/S1/PC-63/2008).

References

[1] R. Rangel, R. Maya-Yescas, R. Garcìa, Catalysis Science & Technology 2 (2012) 639.
[2] B.M. Reddy, A. Khan, P. Lakshmanan, C.L. Cartes, T.C. Rojas, A. Fernandez, Journal of Physical Chemistry B 109 (2005) 1781.
[3] B.M. Reddy, P. Lakshmanan, P. Bharali, P. Saikia, G. Thrimurthulu, M. Muhler, W. Gruenert, Journal of Physical Chemistry C 111 (2007) 10478.
[4] B.M. Reddy, G. Thrimurthulu, L. Katta, Y. Yamada, S.-E. Park, Journal of Physical Chemistry C 113 (2009) 15882.
[5] A. Trovarelli, Comments on Inorganic Chemistry 20 (1999) 263.
[6] A. Migani, G.N. Vayssilov, S.T. Bromley, F. Illasa, K.M. Neyman, Chemical Communications 46 (2010) 5936.
[7] I. Celardo, M.D. Nicola, C. Mandoli, J.Z. Pedersen, E. Traversa, L. Ghibelli, ACS Nano 5 (2011) 37.
[8] W.C. Chueh, C. Falter, M. Abbott, D. Scipio, P. Furler, S.M. Haile, A. Steinfeld, Science 330 (2010) 1797.
[9] N.J. Lawrence, J.R. Brewer, L. Wang, T.-S. Wu, J. Wells-Kingsbury, M.M. Ihrig, G. Wang, Y.-L. Soo, W.-N. Mei, C.L. Cheung, Nano Letters 11 (2011) 2666.
[10] A.K. Sinha, K. Suzuki, Journal of Physical Chemistry B 109 (2005) 1708.
[11] W.C. Mackrodt, M. Fowles, M.A. Morris, US Patent, 4940, p. 685.
[12] L. Liu, X. Wang, M. Guo, M. Zhang, Journal for Nanoscience and Nanotechnology 11 (2011) 2155.
[13] H.P. Klug, L.E. Alexander, X-ray Diffraction Procedures for Polycrystalline and Amorphous Materials, 2nd ed., John Wiley and Sons, New York, 1974.
[14] C. Bozo, F. Gaillard, N. Guilhaume, Applied Catalysis A: General 220 (2001) 69.
[15] B.P. Mandal, V. Grover, A.K. Tyagi, Materials Science and Engineering A 430 (2006) 120.
[16] M.F. García, A.M. Arias, A.I. Juez, C. Belver, A.B. Hungría, J.C. Conesa, J. Soria, Journal of Catalysis 194 (2000) 385.
[17] W.Y. Hernàndez, O.H. Laguna, M.A. Centeno, J.A. Odriozola, Journal of Solid State Chemistry 184 (2011) 3014.
[18] M. Sugiura, Catalysis Surveys from Asia 1 (2003) 77.
[19] L. Li, F. Chen, J.-Q. Lu, M.-F. Luo, Journal of Physical Chemistry A 115 (2011) 7972.
[20] M.-F. Luo, Z.-L. Yan, L.-Y. Jin, Journal of Molecular Catalysis A: Chemical 260 (2006) 157.
[21] B.M. Reddy, L. Katta, G. Thrimurthulu, Chemistry of Materials 22 (2010) 467; R.K. Usmen, G.W. Graham, W.L.H. Watkins, R.W. McCabe, Catalysis Letters 30 (1995) 53.
[22] A. Nakajima, A. Yoshihara, M. Ishigame, Physical Review B 50 (1994) 13297.
[23] M. Guo, J. Lu, Y. Wu, Y. Wang, M. Luo, Langmuir 27 (2011) 3872.
[24] F. Deganello, A. Martorana, Journal of Solid State Chemistry 163 (2002) 527.
[25] H. Borchert, Y.V. Frolova, V.V. Kaichev, I.P. Prosvirin, G.M. Alikina, A.I. Lukashevich, V.I. Zaikovskii, E.M. Moroz, S.N. Trukhan, V.P. Ivanov, E.A. Paukshtis, V.I. Bukhtiyarov, V.A. Sadykov, Journal of Physical Chemistry B 109 (2005) 5728.
[26] P. Fleming, S. Ramirez, J.D. Holmes, M.A. Morris, Chemical Physics Letters 509 (2011) 51.
[27] D.M. Kempaiah, S. Yin, T. Sato, Crystal Engineering Communications 13 (2011) 741.
[28] S. Tsunekawa, R. Sahara, Y. Kawazoe, A. Kasuya, Materials Transactions Online – The Japan Institute of Metals 41 (2000) 1104.
[29] J. Kašpar, P. Fornasiero, M. Graziani, Catalysis Today 50 (1999) 285.
[30] Y.-C. Chen, K.-B. Chen, C.-S. Lee, M.C. Lin, Journal of Physical Chemistry C 113 (2009) 5031.
[31] W. Liu, M.F. Stephanopoulos, Journal of Catalysis 153 (1995) 317.
[32] K.N. Rao, P. Bharali, G. Thrimurthulu, B.M. Reddy, Catalysis Communications 11 (2010) 863.
[33] J.B. Park, J. Graciani, J. Evans, D. Stacchiola, S.D. Senanayake, L. Barrio, P. Liu, J.F. Sanz, J. Hrbek, J.A. Rodriguez, Journal of the American Chemical Society 132 (2010) 356.
[34] S. Yuen, Y. Chen, J.E. Kibsh, J.A. Dumesic, N. Topsøe, H. Topsøe, Journal of Physical Chemistry 86 (1982) 3022.
[35] Y. Chen, L. Zhang, Catalysis Letters 12 (1992) 51.